PROCEEDINGS OF SCIENCE

Particle acceleration and multi-messenger emission from ultra-fast outflows

Enrico Peretti[a,*] **and Markus Ahlers**[a]

[a] *Niels Bohr International Academy, Niels Bohr Institute, University of Copenhagen, Blegdamsvej 17, DK-2100 Copenhagen, Denmark*

E-mail: peretti@nbi.ku.dk

The non-jetted activity of active galactic nuclei (AGN) can result in mildly relativistic and wide opening angle outflows known as ultra-fast outflows (UFOs). UFOs, similar to stellar winds, can develop a bubble structure characterized by an inner wind termination shock and an outer forward shock. During the bubble lifetime, while the forward shock rapidly loses its efficiency in accelerating particles, ideal conditions for stationary acceleration at the wind termination shock can be achieved. We present a model for diffusive shock acceleration at the wind termination shock of UFOs which predicts maximum proton energies extending up to the EeV range. In addition, before escaping the UFO, a sizable fraction of accelerated particles is likely to interact with the highly dense gas and the strong radiation field typical of AGN. We compute the gamma-ray and high-energy neutrino fluxes produced in such inelastic collisions together with the associated escaping flux. We finally discuss the multi-messenger implications of our model in terms of cosmic rays, neutrino and gamma-rays produced in isolated UFOs as well as their cumulative diffuse emission.

38th International Cosmic Ray Conference (ICRC2023)
26 July - 3 August, 2023
Nagoya, Japan

*Speaker

PoS(ICRC2023)361

1. Introduction

Active Galactic Nuclei (AGN) are powerful extra-galactic sources fueled by the accretion activity of supermassive black holes (SMBHs). They have been historically classified as radio-loud and radio-quiet. In addition, depending on the amount of obscuring material located on line of sight, they are also typically categorized as Type 1 (Type 2) when they present broad (only narrow) absorption lines in their spectra [1]. From the physical point of view, AGN can be divided into two main classes: jetted and non-jetted [2]. The former, as their name suggests, are characterized by powerful relativistic and collimated jets. They typically feature strong non-thermal emission which often extends up to high-energy (HE) γ-rays. The latter are dominated by thermal emission and lack of strong jetted activity. They are particularly dim or not radiating at the HE.

Highly ionized mildly relativistic winds, known as Ultra-Fast Outflows (UFOs), have been recently discovered in the hard X-ray spectra of AGN as blue-shifted Fe *XXV-XXVI* absorption lines [3]. These fast AGN winds, characterized by wide opening angle and and high kinetic power ($\dot{E} \lesssim 10^{45}$ erg s^{-1}), are a common feedback of the AGN activity that can be found both in radio-loud [4] and radio-quiet [5] AGN. Observational campaigns highlighted that UFOs are common in active galaxies, while their relatively low absolute number (a few dozen) could be limited due to the current technical limitations of our telescopes [6].

AGN-driven winds, similar to those launched by massive stars [7] and starbursts galaxies [8], develop a bubble structure characterized by an outer forward shock (FS) and an inner wind termination shock (WTS) [9, 10]. The FS of AGN-driven winds has been already proposed as a plausible site for particle acceleration and production of hadronic secondaries such as γ-rays and neutrinos [12–14]. However, the physics and the conditions for efficient particle acceleration has been mostly unexplored so far. In fact, models of wind bubble dynamics show that while the FS decelerates in the external medium losing acceleration efficiency in time, stationary conditions for a strong shock can be found at the WTS [11]. This makes the latter the most ideal site for diffusive shock acceleration (DSA) in AGN winds.

UFOs, as the fastest class of AGN-driven wind, have been hypothesized as promising acceleration site of HE particles. Indeed, recent observations performed with Fermi-LAT showed that UFOs are a new class of γ-ray emitters [15, 16] thereby providing compelling evidence of efficient particle acceleration taking place in such objects.

In this work, we present a model for DSA at the WTS as developed in Ref. [17]. In particular, we focus on the maximum energy achievable in these objects by HE particles and we discuss the associated multi-messenger implications in terms of γ-rays, HE neutrinos and escaping cosmic rays (CRs). In particular, we propose the WTS of UFOs as possible acceleration sites of EeV protons and we discuss the possibility of their contribution to the ultra-high-energy CRs (UHECRs) observed at Earth. The multi-messenger radiation from UFOs presents very interesting properties: HE neutrinos are efficiently produced up to PeV through proton-proton (pp) inelastic collisions, while photopion production (pγ) are responsible for neutrino emission up to $\sim 10^2$ PeV. Interestingly, the associated γ-rays produced at energies beyond 10-10^2 GeV could be efficiently absorbed on the optical-ultraviolet thermal photon field of the AGN. This could make UFOs powerful UHECRs and HE neutrinos being partially opaque to VHE γ-rays.

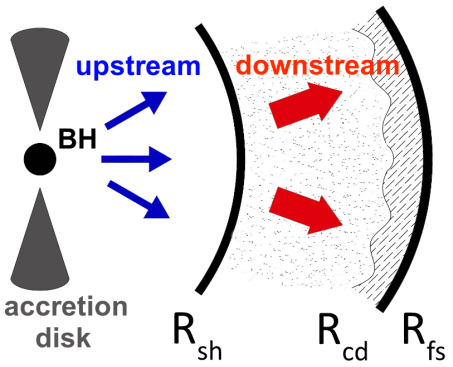

Figure 1: Structure of the wind bubble. The SMBH (BH) responsible for the wind launching is located on the left of the sketch. The blue (red) arrow corresponds to the cool (shocked) wind of the upstream (downstream) region. The wind shock ($R_{\rm sh}$) separates these two regions. The SAM is located between the contact discontinuity ($R_{\rm cd}$) and the forward shock ($R_{\rm fs}$) which bounds the system. Figure from Ref. [17].

2. Model for particle acceleration and multi-messenger radiation

In the following we describe the key aspects characterizing our theoretical model, while for additional details we refer the interested reader to Ref. [17].

A wind bubble forms when a compact source blows a steady supersonic outflow with wide opening angle. Being supersonic, the wind produces a FS launched in the external medium. The impact of the wind material with the external medium leads to the formation of a second shock, the WTS, which is located inside the wind material and it is geometrically reversed, namely its upstream region in the shock rest frame is oriented towards the central engine. The shocked ambient medium (SAM) gets accumulated in a thin shell located immediately behind the FS and it is separated from the shocked wind (SW) by the contact discontinuity (CD). Figure 1 illustrates the structure of the wind bubble where the WTS (located at $R_{\rm sh}$) separates the inner freely expanding wind (blue arrows), hereafter referred to as the upstream region, from the downstream hot shocked wind (red arrows). The CD (identified by $R_{\rm cd}$) separates the SW from the SAM and the FS ($R_{\rm fs}$) bounds the system from the external medium.

The wind bubble evolution proceeds as follows: after an initial phase of free expansion, which ends when the swept-up mass roughly balances the total mass in the wind, the bubble enters the deceleration phase. Under the assumption of an homogeneous external medium of density n_0, during the deceleration the motion of the FWS and the WTS obey the following self-similar relations: $R_{\rm fs} \sim t^{3/5}$ and $R_{\rm sh} \sim t^{2/5}$.

During the deceleration, the WTS decelerates faster than the FS, but keeps the strong jump conditions because the relative speed between the free expanding wind and the shock remains high. In addition, the dynamical timescale of the system becomes soon longer than all timescales associated to HE particles. Therefore, quasi-stationary conditions for the CR transport can be achieved. The FS could be also a potential site for DSA. However, different from the WTS, its acceleration efficiency is expected to rapidly decrease in time while its relative velocity with the external medium drops. Moreover, a high Mach number is not guaranteed at the FS given the unknown temperature of the external medium. On the other hand the free expanding wind has time

Parameter	benchmark	A	B	C
u_1/c	0.2	-	-	-
$\dot{M}[\mathrm{M}_\odot\,\mathrm{yr}^{-1}]$	10^{-1}	-	-	-
ξ_{CR}	0.05	0.087	0.1	0.12
ϵ_{B}	0.05	-	-	-
$l_c\,[\mathrm{pc}]$	10^{-2}	-	-	-
δ	3/2	-	-	-
$L_X[\mathrm{erg\,s}^{-1}]$	10^{44}	-	-	-
$n_0[\mathrm{cm}^{-3}]$	10^4	$2\cdot10^3$	$5\cdot10^2$	$2\cdot10^2$
$t_{\mathrm{age}}\,[\mathrm{yr}]$	10^3	$3\cdot10^3$	10^4	$2\cdot10^4$

Table 1: Parameters of the benchmark UFO and of the three alternative scenarios considered for the multi-messenger emission.

to cool adiabatically before it reaches the WTS.

In this context, we model the DSA at the WTS and the CR transport in the wind bubble assuming stationary conditions for HE particles and spherical symmetry. We assume the following boundary conditions: 1) no (re-)acceleration and free escape at the FS; 2) zero net flux at $r = 0$. DSA can take place efficiently at the WTS. Therefore the following injection term is assumed:

$$Q(r,p) = Q_0(p)\delta[r - R_{\mathrm{sh}}] = \frac{\eta_{\mathrm{CR}} u_1 n_1}{4\pi p^2}\delta[p - p_{\mathrm{inj}}]\delta[r - R_{\mathrm{sh}}], \tag{1}$$

where $p_{\mathrm{inj}} = 1$ GeV/c is the injection momentum, while n_1 and u_1 are, respectively, the gas density and speed immediately upstream of the WTS. The transport equation we solve is the following:

$$r^2 u \partial_r f = \partial_r[r^2 D \partial_r f] + \frac{p}{3}\partial_p f\, \partial_r[r^2 u] + r^2[Q - \lambda f]\,, \tag{2}$$

where $u = u(r)$ is the wind profile, $D = D(r,p)$ is the diffusion coefficient, $Q = Q(r,p)$ is the injection term and $\lambda = \lambda(r,p)$ is the loss rate accounting for pp and pγ interactions. The wind radial profile is constant in the upstream region while, assuming that the UFO dynamics is energy-conserving, the downstream velocity scales as r^{-2}. Accordingly, the gas density is constant in the downstream ($n_2 = 4n_1$) and it scales as r^{-2} in the upstream. The diffusion coefficient is computed in the context of quasi-linear theory assuming a Kraichnan-like index ($\delta = 3/2$) for the turbulent cascade, and a coherence length l_c. We additionally take into account the transition in the diffusion coefficient from the resonant scattering regime to the small pitch angle scattering regime which takes place when the CR Larmor radius exceeds l_c. Finally, the magnetic field is assumed to be of turbulent nature and its normalization is fixed by the requirement that the magnetic field pressure in the upstream region is a fraction $\epsilon_B \lesssim 10\%$ of the ram pressure.

We assume that $R_{\mathrm{cd}} \simeq 0.9 R_{\mathrm{fs}}$ and we assume no mixing between the SW and the SAM. The SAM density therefore is roughly $n_{\mathrm{SAM}} \simeq 4n_0$. The thermal AGN photon field is assumed to scale as r^{-2} from the centrum and it comprises the optical-ultraviolet big blue bump and hard X-ray power-law emission as described in Ref. [18]. We consistently consider the infrared photon field of the dusty torus as described in Ref. [19].

We solve the transport with the semi-analytic iterative algorithm described in Ref. [17] and we refer to this reference for further details. The general form of the solution at the WTS reads:

$$f_{\mathrm{sh}}(p) = C p^{-s} \mathrm{e}^{-\Gamma_{\mathrm{cut}}(p)}, \tag{3}$$

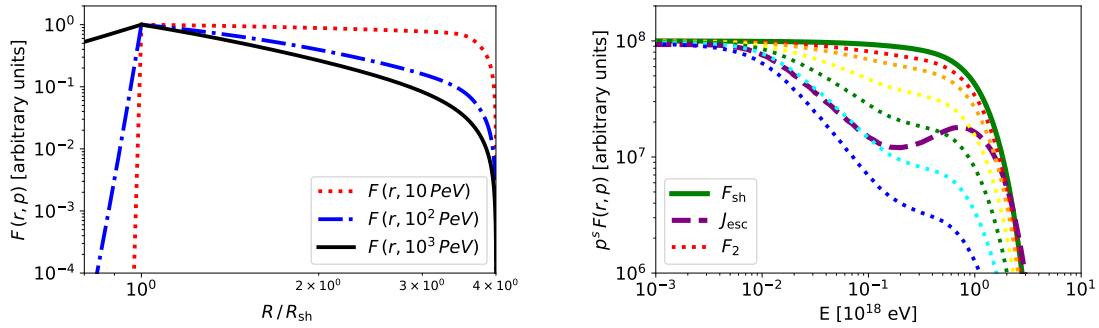

Figure 2: Top panel: Spatial distribution of the CR phase space density. We show the results for three representative CR energies: $E = 10$ PeV (red dotted line), $E = 100$ PeV (blue dashed line), and $E = 1$ EeV (black solid line). **Bottom panel:** Spectrum of particles at the shock (thick green line) compared to the spectral shape of the escaping flux (dashed magenta line). The dotted curves represent the particle spectra in the downstream region. From red to blue the dotted lines are computed at $r/R_{\rm fs} = 0.29$, 0.33, 0.44, 0.57, 0.75, and 0.9.

where C is a normalization constant, s is the spectral index ($s = 4$ in strong shocks) and $\Gamma_{\rm cut}(p)$ is a HE cut-off function which includes energy losses and escape. The normalization constant C is computed in the test-particle regime which is ensured by assuming that the CR pressure at the shock is a fraction $\xi_{\rm CR} \lesssim 10\%$ of the ram pressure.

The CR phase space density is determined at every radius r using Eq. (2), and this allows us to compute the emissivity of γ-rays and neutrinos resulting from pp [20] and pγ [21] interactions. We account for $\gamma\gamma$ absorption inside the wind bubble as well as on the EBL [22] for γ-rays *en route* to Earth. We finally compute the flux of escaping CRs at the forward shock as $j_{\rm esc} = -D\partial_r f|_{R_{\rm fs}}$.

3. Results

In order to discuss the results of our model we assume a set of parameters, hereafter referred to as the *benchmark scenario*. The set of parameters of the benchmark scenario are listed in Table 1 (second column). Those not already defined are the following: the terminal wind speed u_1, the mass loss rate $\dot{M}$, the X-ray luminosity L_X and the age of the system $t_{\rm age}$.

The left panel of Figure 2 illustrates the radial distribution of CRs in the system for the benchmark scenario. The three curves, from red (low energy) to blue (intermediate energy) and black (highest energy), highlight the behavior of CRs of respectively different energy in the system. In particular, in the upstream region ($r/R_{\rm sh} < 1$), low energy particles are forced by the advection to be confined in the immediate vicinity of the WTS, whereas the higher the energy the wider is the spread towards the central engine due to diffusion. Such a behavior can be qualitatively understood in terms of the upstream diffusion length, D_1/u_1, namely the higher the energy the wider is the typical distance that particles can back-stream. The downstream region ($r/R_{\rm sh} > 1$) is characterized by a dominant role of advection at low energy while the highest energy CRs diffuse efficiently away from the system. The escape makes the radial distribution of the highest energy particles approaching asymptotically the r^{-1} behavior typical of 3D diffusion under stationary conditions.

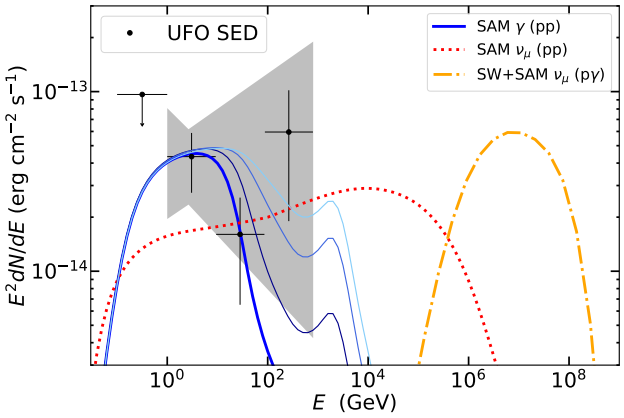

Figure 3: Gamma-ray (thick blue line) and HE neutrino flux produced in the benchmark UFO ($R_{\rm sh} \simeq 0.8$ pc) via pp (dotted red line) and pγ (orange dot-dashed line) interactions. The acronym SAM (SW) refers to the shocked ambient medium (shocked wind). The thin blue-to-cyan lines represents the γ-ray flux computed, respectively, for scenario A, B and C (see Table 1) in order to illustrate the dependence of the γ-ray absorption on the bubble expansion (where $R_{\rm sh} \simeq 2$, 5 and 8 pc, respectively). The UFO is assumed to be located at z=0.013 in order to be directly compared with the best-fit UFO SED provided in Ajello et al. [15], where the gray band represent the 1 σ uncertainty band of such a best-fit UFO SED.

The right panel of Figure 2 shows and compares the spectrum of CRs accelerated at the WTS (solid green) with that of the escaping flux (dashed violet). The spectrum at the shock presents the typical DSA power law p^{-4} up to a maximum energy $E_{\rm max} \simeq 1$ EeV. The escaping flux follows the spectrum of the accelerated particles up to 10 PeV. In the energy range from 10 PeV up to 200 PeV it features a dip due to pγ energy losses on the optical-ultraviolet field of the AGN becoming more relevant than the escape. Finally, at the highest energies the spectrum of the escaping flux hardens because the escape dominates over energy losses. The dotted lines, from red to blue, illustrate the spectrum computed at different radii in the downstream region, respectively, from the shock vicinity to the contact discontinuity. They are computed in order at $r/R_{\rm fs} = 0.29$, 0.33, 0.44, 0. 57, 0.75, and 0.9, while $R_{\rm sh}/R_{\rm esc} \simeq 0.25$. Notice that while moving from the WTS to the FS, the spectrum softens due to the combined effects of energy losses and escape.

Figure 2 shows the γ-ray and associated HE neutrino spectra produced in UFOs. Here, the γ-ray spectrum produced in the benchmark scenario (solid blue curbe) is compared with alternative scenarios, A, B and C (see Table 1) having identical power but different environmental conditions and age. The spectra are also compared with the UFO spectrum inferred from the stacking analysis performed by the Fermi-LAT Collaboration [15]. One can see that our model can well reproduce the power as well as the spectral behavior inferred from observations. Notice, in particular, that the different scenarios are characterized by different levels of $\gamma\gamma$ absorption in the source due to a variation in size of the system which, in turn, results in a spectrum fading from 10 GeV in the benchmark scenario to a few TeV in scenario C. The red dotted and yellow dot-dashed lines represent the single-flavor neutrino flux, respectively, resulting from pp and pγ interactions. The pp spectrum extends roughly up to 10^2 TeV while the pγ components dominate the emission up to 10^2 PeV. Interestingly, such a neutrino flux, depending on the specific scenario considered, might come with a partially absorbed multi-GeV or TeV γ-ray counterpart.

UFOs are common in nearby active galaxies and are observed, both, in radio-loud and radio-quiet AGN, thereby suggesting that they could be ubiquitous in all AGN types, from Seyfert galaxies to blazars. In order to assess their possible contribution as diffuse sources we assume that the benchmark scenario is an UFO standard candle and a good representative for such a source class. The CR luminosity of an UFO reads:

$$L_{\rm CR} \simeq 2 \cdot 10^{43} \eta_{\rm loss} \left(\frac{\xi_{\rm CR}}{0.05}\right) \left(\frac{\dot{M}}{10^{-1} {\rm M}_\odot \, {\rm yr}^{-1}}\right) \left(\frac{u_1}{0.2c}\right)^2 \, {\rm erg \, s}^{-1} \, , \tag{4}$$

where $\eta_{\rm loss}$ is an age dependent parameter of order unity quantifying the impact of energy losses in the escaping flux. By assuming a local comoving source density of $\rho_0 \simeq 10^{-5} \, {\rm Mpc}^{-3}$ typical of AGN with X-ray luminosity of $L_X \simeq 10^{44} \, {\rm erg \, s}^{-1}$ [23], we estimate the order of magnitude of the flux of UHECRs and HE neutrinos from UFO following the formalism developed in Ref. [24]. In particular, the UHECR flux reads:

$$[E_p^2 \phi_{\rm CR}]_{\rm EeV} \simeq 3 \cdot 10^{-7} \left(\frac{\rho_0}{10^{-5} \, {\rm Mpc}^{-3}}\right) \left(\frac{\xi_z}{2.6}\right) \left(\frac{L_{\rm CR}}{10^{43} {\rm erg \, s}^{-1}}\right) \frac{\rm GeV}{\rm cm^2 s \, sr} \, . \tag{5}$$

The associated neutrino flux is:

$$E_\nu^2 \phi_{{\rm all}\nu} \simeq 2 \cdot 10^{-8} \left(\frac{\rho_0}{10^{-5} {\rm Mpc}^{-3}}\right) \left(\frac{\xi_z}{2.6} \frac{n_0}{10^4 {\rm cm}^{-3}}\right) \left(\frac{t_{\rm age}}{10^3 {\rm yr}}\right) \left(\frac{L_{\rm CR}}{10^{43} {\rm erg \, s}^{-1}}\right) \frac{\rm GeV}{\rm cm^2 s \, sr} \, , \tag{6}$$

where $\xi_z = 0.5, 2.6, 7.8$ for flat, star-formation-rate, and AGN redshift distributions of sources, respectively.

Interestingly, we note that the order of magnitude of the multi-messenger flux from UFOs is comparable with the current measures of UHECRs at EeV and HE neutrinos at PeV performed, respectively, by the Pierre Auger Observatory [25] and IceCube [26].

4. Conclusions

Ultra-Fast Outflows (UFOs) are the fastest known AGN-driven winds observed in the core of active galaxies. In this work we present a model discussing whether diffusive shock acceleration can take place efficiently at the wind termination shock of UFOs. We showed that energies up to EeV could be achieved by protons in these sources making UFOs promising candidates for UHECR accelerators. We refer the interested reader to Ref. [17] for a discussion on the impact of different parametric assumption on the maximum energy.

UFOs are characterized by high gas and photon densities and the production of γ-rays as well as high energy neutrinos could take place efficiently. In particular, we showed that UFOs could be powerful PeV neutrino emitters with a partially absorbed γ-ray counterpart depending on the size of the wind bubble.

In addition, UFOs are also interesting sources for the multi-messenger diffuse flux of UHECRs and HE neutrinos. We showed that, under standard parametric assumptions, UFOs could dominate the multi-messenger diffuse flux currently observed by the Pierre Auger Observatory at EeV and at PeV by IceCube.

Acknowledgements.—The research activity of EP and MA was supported by Villum Fonden (project No. 18994). EP was also supported by the European Union's Horizon 2020 research and innovation program under the Marie Sklodowska-Curie grant agreement No. 847523 'INTERACTIONS'.

References

[1] Urry C. M., Padovani P., 1995, PASP, 107, 803.

[2] Padovani P., 2017, NatAs, 1, 0194.

[3] Tombesi F., et al., 2010, A&A, 521, A57.

[4] Tombesi F., et al., 2014, MNRAS, 443, 2154.

[5] Tombesi F., et al., 2012, MNRAS, 422, L1.

[6] Laha S., et al., 2021, NatAs, 5, 13.

[7] Morlino G., et al., 2021, MNRAS, 504, 6096.

[8] Peretti E., et al., 2022, MNRAS, 511, 1336.

[9] Weaver R., et al., 1977, ApJ, 218, 377.

[10] Koo B.-C., McKee C. F., 1992, ApJ, 388, 93.

[11] Faucher-Giguère C.-A., Quataert E., 2012, MNRAS, 425, 605.

[12] Lamastra A., et al., 2016, A&A, 596, A68.

[13] Wang X., Loeb A., 2017, PhRvD, 95, 063007.

[14] Liu R.-Y., et al., 2018, ApJ, 858, 9.

[15] Ajello M., et al., 2021, ApJ, 921, 144.

[16] Peretti E.,et al., 2023, arXiv, arXiv:2303.03298.

[17] Peretti E., et al., 2023, arXiv, arXiv:2301.13689.

[18] Marconi A., et al., 2004, MNRAS, 351, 169.

[19] Mullaney J. R., et al., 2011, MNRAS, 414, 1082.

[20] Kelner S. R., et al., 2006, PhRvD, 74, 034018.

[21] Kelner S. R., Aharonian F. A., 2008, PhRvD, 78, 034013.

[22] Franceschini A., Rodighiero G., 2017, A&A, 603, A34.

[23] Fiore F., et al., 2017, A&A, 601, A143.

[24] Ahlers M., Halzen F., 2018, PrPNP, 102, 73.

[25] Aab A., et al., 2018, ApJL, 853, L29.

[26] Abbasi R., et al., 2022, ApJ, 928, 50.